# Design of Optimal Velocity Tracking Controllers
# for One and Two-Body Point Absorber Wave Energy Converters

Adam Stock[a,*], Carlos Gonzalez[b]

[a]*Wind Energy and Control Centre, Department of Electrical and Electronic Engineering, University of Strathclyde, G1, 1XQ, Scotland, UK*
[b]*Renewable Dynamics Ltd, 50 Richmond Street, Glasgow, G1 1XP, Scotland, UK*

## Abstract

Point absorber Wave Energy Converters (WECs) are typically operated using linear damping control in which the resistive force of the power take-off (PTO) is linearly proportional to the velocity of the floater. Such algorithms are used predominantly due to their simplicity and ease of application, however, it is known that such control is far from optimal in terms of energy capture. Previous studies in the literature have seen a number of different, more advanced control methodologies proposed, however, in the main, these have been applied to single body point absorbers. In this paper, an Optimal Velocity Tracking (OVT) controller is designed using a novel controller design model and applied to a WEC-Sim model of a utility scale single-body point absorber. The methodology is then extended to the two-body point absorber WEC case and an OVT controller is designed for a utility scale two-body WEC. The increase in energy capture for a site in UK waters, based on WEC-Sim simulations and compared to typical linear damping control, is found to be 23% for the one-body WEC and 20% for the two-body WEC.

*Keywords:* Wave Energy, Control, Ocean Energy

## 1. Introduction

Conversion of wave energy to useful energy (usually in the form of electrical energy) has been studied for several decades, with many different wave energy converter (WEC) designs proposed over this time [1, 2]. One common form of WEC is a point absorber, a device that is typically small in comparison the wave length, which in turn results in the WEC having a narrow bandwidth. As a WEC will typically have to operate off resonance, control is of particular importance for point absorber (or other narrow bandwidth) devices [3]. In order to efficiently convert energy away from the resonant frequency, control algorithms can be used that typically employ the power take-off (PTO) as the actuator. It has been shown that the optimum method for control of a point absorber is via impedance matching control [4], however, this is almost impossible to achieve without highly accurate wave forecasting due to the acausal nature of the control problem. Several different approaches have been discussed in the literature that use approximations to impedance matching. These include Model Predictive Control (MPC), Approximate Complex Conjugate Control (ACC) and Optimal Velocity Tracking (OVT). Whilst these methodologies have all been explored in the literature (e.g. [3, 5]), work has typically focused on the single body case (see [6]), i.e. whereby one end of the PTO is in a fixed position, with only limited research into impedance matching control for two-body devices (e.g. [7, 8, 9, 10]). In particular, to the authors' knowledge, OVT has not been applied to the two-body case in the literature. This work

---

*Corresponding author
  *Email addresses:* `adam.stock@strath.ac.uk` (Adam Stock), `carlos.gonzalez@renewable-dynamics.com` (Carlos Gonzalez)
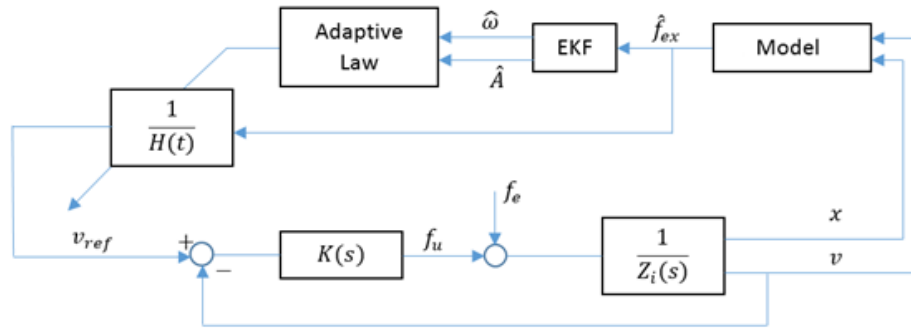
Figure 1: Schematic of Optimal Velocity Tracking control based on the Fusco and Ringwood methodology

therefore aims to fill this gap in the literature by presenting a methodology for designing OVT controllers for two body devices, including demonstration of the controller via simulation in the industry standard WEC-Sim simulation software [11].

In section 2 the methodology for designing OVT controllers is discussed. The methodology for a single body WEC is first presented and applied in subsection 2.1 in order to outline the general concept before being extended to the two body case in subsection 2.2. In section 3 the controllers for each WEC are designed for example utility scale WECs, with simulation results comparing performance to linear damping control presented in section 4.

## 2. Methodology

In this section the methodology for design of OVT controllers for two-body WECs is presented. Firstly, in subsection 2.1, the Integrated Marine Point Absorber Control Tool (IMPACT) is discussed in the context of a single body WEC. Extension of IMPACT for two-body point absorbers is then discussed in subsection 2.2 and the incorporation of limits on the PTO is discussed in subsection 2.3.

### 2.1. OVT for a Single Body WEC

The Integrated Marine Point Absorber Control Tool (IMPACT) [12] is intended for use in designing and implementing controllers for point absorber devices. IMPACT is comprised of a controller design methodology and an OVT controller structure that, when used together, allow OVT controllers to be designed and implemented for point absorber WECs. The tool requires the input of the basic WEC information, which is used to create frequency domain models based on the Cummins equation. The frequency domain models can then be used to generate approximations of the WEC dynamics, useful for prediction of the wave dominant frequency and excitation force on the WEC bodies, and to allow design of the OVT controller. The OVT controller structure that is used is an extension of that proposed in [5].

### 2.1.1. Controller structure

The OVT controller structure is shown diagrammatically in Fig. 1. With reference to Fig. 1, the plant is represented as the reciprocal of the intrinsic impedance $Z_i$, with measurements of the position and speed ($x$ and $v$ respectively) outputted. A model is used to calculate an estimate of the excitation force $\hat{f}_{exc}$, which is in turn input to an Extended Kalman Filter (EKF), which provides estimates of the dominant wave frequency $\hat{\omega}$ and the wave amplitude $\hat{A}$. An adaptive law based on the dynamics of the WEC ($H(t)$) is then used to scale the excitation force and hence produce a reference velocity $v_{ref}$ that is compared to the measured velocity to produce an error fed into the tracking controller $K(s)$. The output of the controller is the useful force of the PTO $f_u$, which, when combined with the excitation force on the WEC completes the loop back to the plant.
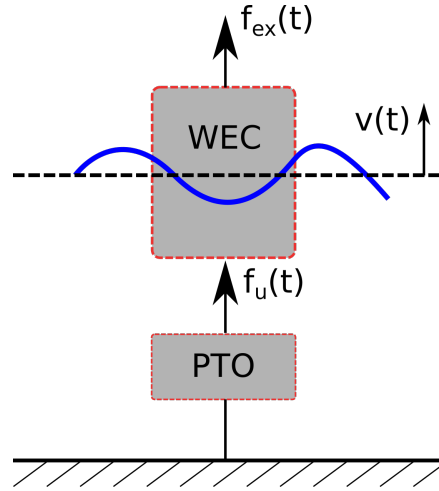
Figure 2: Single body point absorber with PTO

### 2.1.2. Adaptive Law

Consider the system shown in Fig. 2. Using the Cummin's equation, the dynamics can be described by,

$$F_{exc}(j\omega) + F_u = -\omega^2(M + A(\omega))Q(j\omega) + j\omega B(\omega)Q(j\omega) + CQ(j\omega) \tag{1}$$

where M is the mass of the WEC, $A(\omega)$ is the added mass (given by $M_A(\omega) + M_\infty$, which is the added mass plus the infinite added mass, Q is the generalised position vector (assumed to be a sine wave with the same frequency but different amplitude and and phase), $B(\omega)$ is the frequency dependant damping matrix, and $C$ is the restoring force. Assuming motion only in heave with velocity $V(\omega)$, equation 1 can be rewritten more succinctly with velocity as the subject such that,

$$V(\omega) = \frac{1}{Z_i(\omega)}(F_{exc}(\omega) + F_u(\omega)) \tag{2}$$

where the intrinsic impedance $Z_i$ is defined as,

$$Z_i(\omega)) = B(\omega) + j\omega\Big(M_A(\omega) + M_\infty - \frac{C}{\omega^2}\Big) \tag{3}$$

Maximum energy extraction occurs when,

$$F_u(\omega) = -Z_i^*(\omega)V(\omega) \tag{4}$$

or, equivalently, when

$$V(\omega) = \frac{1}{Z_i(\omega) + Z_i^*(\omega)}F_{exc} = \frac{1}{2B(\omega)}F_{exc} \tag{5}$$

where $^*$ indicates the complex conjugate[1]. It is clear that $\frac{1}{2B(\omega)}$ can be thought of as the ratio between velocity and excitation force in the frequency domain.

Notably, $\frac{1}{2B(\omega)}$ is non-causal, however, as highlighted in [5] the non-causality is the result of the fact that all frequencies may be present at once, but, because the relationship between frequency and $\frac{1}{2B(\omega)}$ is in fact quite flat over a broad range of frequencies and because the excitation force tends to be contained within a constrained band of frequencies a causal approximation is appropriate. In the time domain this means that a value of $1/2B(\omega)$ at a given time $t$, defined as $H(t)$ can be looked up using the peak frequency of excitation and the reference velocity $v_{ref}(t)$ can be found via,

$$v_{ref}(t) = \frac{1}{H(t)}f_{exc} \tag{6}$$

---

[1]proofs are readily available in the literature, notably in [4]

In order to calculate the reference velocity using the adaptive law an estimate of the dominant frequency of the excitation $\hat{\omega}$ is required. Note that for the limits discussed in section 2.3 an estimate of the excitation amplitude is also required, hence its inclusion in Fig. 1. The estimates of the dominant excitation frequency and amplitude are, in this case, provided by an Extended Kalman Filter (EKF) that i sprovided with an estimate of the excitation force on the WEC. Note that it is feasible to use other methodologies to provide the dominant excitation frequency and amplitude if desired.

### 2.1.3. Extended Kalman Filter (EKF)

Given a linear dynamic system in a state space representation, with state vector $x_k$, input vector $u_k$, measured output vector $y_k$ and system and output noise vectors $w_k$ and $v_k$ respectively represented by the following equations

$$x_{k+1} = A \cdot x_k + B \cdot u_k + w_k \tag{7}$$

$$y_k = H \cdot x_k + v_k \tag{8}$$

a Kalman filter is an algorithm that provides the values of the states that minimise the error covariance. The error is defined as the difference between the real and estimated values of the state vector such that

$$e_k = x_k - \hat{x}_k \tag{9}$$

and the covariance matrix $P$ is defined by

$$P_k = E(e_k \cdot e_k^t) \tag{10}$$

The output and system covariance matrices $R$ and $Q$ are defined by

$$Q_k = E(v_k \cdot v_k^t) \tag{11}$$

$$R_k = E(w_k \cdot w_k^t) \tag{12}$$

The Extended Kalman Filter provides the estimates of the state vector on the non-linear system:

$$\begin{aligned} x_{k+1} &= f(x_k, u_k) \\ z_{k+1} &= h(x_k, u_k) \end{aligned} \tag{13}$$

following the algorithm given by

$$\begin{aligned} \hat{x}_{k+1|k} &= f(x_k, u_k) \\ P_{k+1|k} &= F_x P_k F_x^T + Q_k \\ K_{k+1} &= P_{k+1|k} H_{k+1}^T (H_{k+1} \\ P_{k+1|k} H_{k+1}^T + R_{k+1})^{-1} \\ x_{k+1} &= \hat{x}_{k+1|k} + K_{k+1}\left(z_{k+1} - h(\hat{x}_{k+1|k})\right) \\ P_{k+1} &= (I - K_{k+1} H_{k+1}) P_{k+1|k} \end{aligned} \tag{14}$$

where

$$F_x = \partial f / \partial x$$

is the jacobian of $f$.

The model for the extended Kalman filter is a cyclical model in which the frequency changes slowly. The measured signal is represented by the state variable $\psi$. The model in discrete form is given by

$$\begin{bmatrix} \psi(k+1) \\ \psi^*(k+1) \\ \omega(k+1) \end{bmatrix} = \begin{bmatrix} \cos\omega(k)T_s & \sin\omega(k)T_s & 0 \\ -\sin\omega(k)T_s & \cos\omega(k)T_s & 0 \\ 0 & 0 & 1 \end{bmatrix} \begin{bmatrix} \psi(k) \\ \psi^*(k) \\ \omega(k) \end{bmatrix} + \begin{bmatrix} \epsilon(k) \\ \epsilon^*(k) \\ \kappa(k) \end{bmatrix} z(k) = \begin{bmatrix} 1 & 0 & 0 \end{bmatrix} \begin{bmatrix} \psi(k+1) \\ \psi^*(k+1) \\ \omega(k+1) \end{bmatrix} + v(k) \tag{15}$$

where input noise disturbances $w_k$ are represented by $\epsilon(k)$ and $\epsilon^*(k)$, and the variability in frequency $\omega(k)$ is represented by a random walk model (driven by the white noise $\kappa(k)$). The required functions/matrices are therefore given by

$$f(x_k, u_k) = \begin{bmatrix} \cos \omega(k)T_s & \sin \omega(k)T_s & 0 \\ -\sin \omega(k)T_s & \cos \omega(k)T_s & 0 \\ 0 & 0 & 1 \end{bmatrix} \begin{bmatrix} \psi(k) \\ \psi^*(k) \\ \omega(k) \end{bmatrix} H(x_k, u_k) = \psi \tag{16}$$

$$F_x = \begin{bmatrix} \cos \omega_k T_s & \sin \omega_k T_s & -T_s \sin \omega_k T_s \psi_k + T_s \cos \omega_k T_s \psi_k^* \\ \sin \omega_k T_s & \cos \omega_k T_s & -T_s \cos \omega_k T_s \psi_k - T_s \sin \omega_k T_s \psi_k^* \\ 0 & 0 & 1 \end{bmatrix} H_k = \begin{bmatrix} 1 & 0 & 0 \end{bmatrix} \tag{17}$$

The value of $z_k$ is provided through an estimation of the excitation force detailed in subsection 2.1.4. The application of the EKF used here is not the usual application of a Kalman filter, which is usually used for cases where there is a physical system with noise sensors and the values of the covariance matrices are related to the noise of the measured variable. Although there is noise in the sensors used to estimate the excitation force, the main component of the error is the fact that the input to the EKF is a not a pure cyclical signal, therefore the value for the output covariance is the order of the magnitude of the square of the excitation force ($10^8$ to $10^{12}$). The error in modelling of the system is given by the system covariance. The frequency is assumed to change very slowly and hence the value for its system covariance is quite small. Values between $10^{-8}$ and $10^{-12}$ good gives results. Errors of 1% of the excitation force can be assumed for $\psi$ and $\psi^*$. This gives a covariance of between $10^5$ and $10^6$. The smaller the values of the system covariances, the smoother the output signals are.

### 2.1.4. Estimation of the Excitation Force

An estimate of the excitation force can be provided based upon a model of the WEC intrinsic impedance, with the position, velocity and acceleration of the WEC used as inputs. The model used is based upon the dynamics described by the Cummins equation, whereby

$$(M + A_\infty)\ddot{q} + \int_0^t K(t - \tau)\dot{q}(\tau)d\tau + Cq - F_u = F_{exc} \tag{18}$$

The convolution integral is computationally expensive and it can be approximated by a state space model. In an equivalent way, the numerical magnitude and phase of the frequency response are found and then an approximate transfer function is found by using the methodology described in [13]. In some cases, the dynamics can be represented by a second order system that is equivalent to

$$F_{exc} = M\ddot{q} + B\dot{q} + Cq - F_u \tag{19}$$

More typically, higher order models are required to accurately model the WEC's behaviour. In these cases, the dynamics can be split into a high order transfer function $H_{HO}$ which multiplies the acceleration, velocity and position terms such that,

$$F_{exc} = \left( \frac{1}{H_{HO}}(Ms^2 + Bs + C)q \right) - F_u \tag{20}$$

In this case the measured acceleration is multiplied by M, the measured velocity by B and the measured displacement by K and then filtered through the transfer function $\frac{1}{H_{HO}}$.

### 2.2. Adaptation for Two Body Devices

For single body WECs, the excitation force on a single body is required relative to a stationary point is required to be estimated to allow the EKF to estimate the dominant excitation frequency that is input to the adaptive law. For two-body WECs the dynamics are more complicated, with the relative motion between two bodies requiring to be estimated and the dominant excitation frequency of the bodies relative to one another being output from the EKF. As such, the the method for estimating the excitation force requires adaptation.
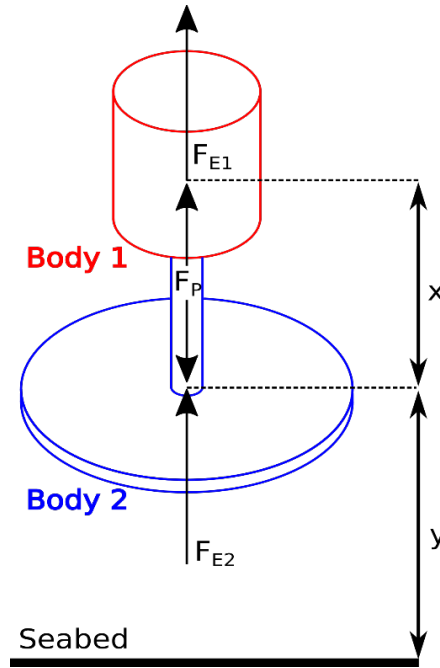
Figure 3: Two Body WEC diagram

### 2.2.1. Estimation of the Excitation Force for Two-Body WECs

With reference to 3, in order to apply the OVT control system to a two-body WEC, the combined dynamics of the floater and spar must be considered. The energy in a two body WEC is produced by the relative movement between the floater (body 1) and the spar (body 2). The equations of motion of the two bodies are combined to give a single equation for the dynamics of the system that links the relative movement ($x$) to the PTO force and the excitation forces on the floater ($F_{E1}$) and the spar ($F_{E2}$).

First, considering body 1, the dynamics are given by

$$(M_1 + A_1)(\ddot{y} + \ddot{x}) + D_1(\dot{y} + \dot{x}) + k_1(y + x) = F_{e1} + F_P \tag{21}$$

where $M_1$ is the mass of the body, $A_1$ is the added mass term, $D_1$ represents the radiation term, and $k_1$ represents the restoring force term. These terms are functions of frequency, the ($\omega$) notation is omitted for ease of reading. The excitation force is $F_E 1$ and the PTO force is $F_P$. Considering now just the spar (body 2),

$$(M_2 + A_2)(\ddot{y}) + D_2\dot{y} + k_2 y = F_{e2} - F_P \tag{22}$$

A simpler and equivalent formulation for body 1 and body 2 respectively is,

$$Z_1(\omega)(\dot{x} + \dot{y}) = F_{E1} + F_P \tag{23}$$

$$Z_2(\omega)\dot{y} = F_{E2} - F_P \tag{24}$$

where $Z_1$ and $Z_2$ represent the impedance of the floater and spar in isolation. An expression for the relative motion of the two bodies in a similar form to the single body case can be derived by combining the equations such that,

$$\hat{Z}\dot{x} = \hat{F}_E + F_P \tag{25}$$

where $\hat{Z}$ and $\hat{F}_E$ are the equivalent impedance and force of the system respectively. From equation 24,

$$\dot{y} = \frac{F_{E2} - F_P}{Z_2} \tag{26}$$

6

Inserting into equation 23 and then rearranging yields,

$$\frac{Z_1 Z_2}{Z_2 + Z_1} \dot{x} = \frac{Z_2}{Z_2 + Z_1} F_{E1} - \frac{Z_1}{Z_2 + Z_1} F_{E2} + F_P \tag{27}$$

Hence the equivalent impedance $\hat{Z}$ from equation 25 is given by,

$$\frac{1}{\hat{Z}} = \frac{1}{Z_1} + \frac{1}{Z_2} \rightarrow \hat{Z} = \frac{Z_1 Z_2}{Z_2 + Z_1} \tag{28}$$

and the equivalent excitation force $\hat{F}_E$ is given by

$$\hat{F}_E = \frac{Z_2}{Z_2 + Z_1} F_{E1} - \frac{Z_1}{Z_2 + Z_1} F_{E2} \tag{29}$$

As discussed in subsection 2.1.2, the optimum velocity $V_{ref}$ is given by

$$V_{ref}(\omega) = \frac{F_E}{2B(\omega)} \tag{30}$$

where $B$ is the radiation resistance (the real component of the impedance). Using the same logic, for the two body case the reference velocity is given by

$$V_{ref}(\hat{\omega}) = \frac{\hat{F}_E}{2|\hat{Z}(\hat{\omega})|cos(\psi(\hat{\omega}))} \tag{31}$$

where $\psi$ is the phase of the impedance and both the impedance and the phase are functions of the combined excitation force frequency $\hat{\omega}$.

### 2.2.2. Body to Body Interaction

The formulation presented in subsection 2.2.1 is a summation of the dynamics of the two bodies and does not include interactions between the bodies. Of course in reality the bodies interact as the movement of one body radiates a wave that in turn induces a force on the other body. The interaction between the two bodies is added by introducing additional terms (a radiation and added mass term) in the dynamics for each body such that,

$$Z_1(\dot{x} + \dot{y}) = F_{E1} + F_P + Z_{21}\dot{y} \tag{32}$$

$$Z_2\dot{y} = F_{E2} - F_P + Z_{12}(\dot{x} + \dot{y}) \tag{33}$$

where $Z_{21}$ and $Z_{12}$ are the force induced by body 2 on body 1 and vice versa respectively. By following similar steps to before to find an equation in the form $\hat{Z}\dot{x} = \hat{F}_E + F_P$, it is clear that,

$$\frac{Z_1 Z_2 - Z_{21} Z_{12}}{Z_1 + Z_2 - Z_{12} - Z_{21}} \dot{x} = \frac{Z_2 - Z_{12}}{Z_1 + Z_2 - Z_{12} - Z_{21}} F_{E1} - \frac{Z_1 - Z_{21}}{Z_1 + Z_2 - Z_{12} - Z_{21}} F_{E2} + F_P \tag{34}$$

Hence, for the model including body to body interactions the equivalent impedance $\hat{Z}$ is given by

$$\hat{Z} = \frac{Z_1 Z_2 - Z_{21} Z_{12}}{Z_1 + Z_2 - Z_{12} - Z_{21}} \tag{35}$$

and the equivalent excitation force $\hat{F}_E$ is given by

$$\hat{F}_E = \frac{Z_2 - Z_{12}}{Z_1 + Z_2 - Z_{12} - Z_{21}} F_{E1} - \frac{Z_1 - Z_{21}}{Z_1 + Z_2 - Z_{12} - Z_{21}} F_{E2} \tag{36}$$

As in the case with no body to body interaction the reference velocity can be found via equation 31.
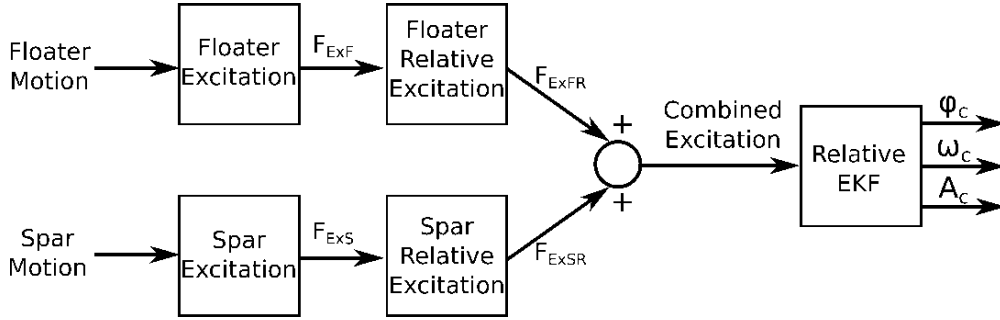
Figure 4: Flow of signals for estimation of relative phase, frequency, and amplitude
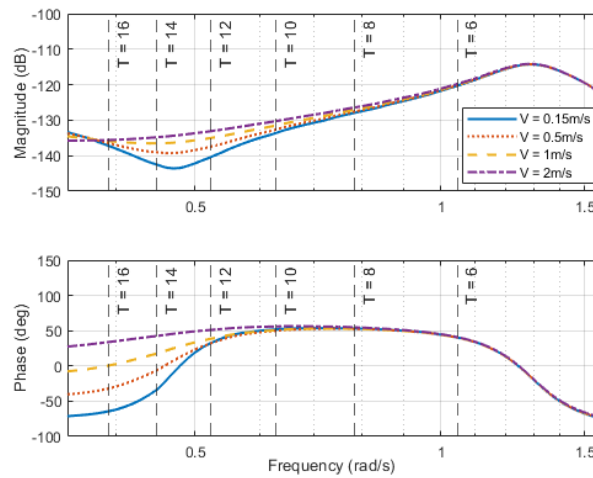


Figure 5: Variation in admittance with velocity for the two-body WEC

### 2.2.3. Excitation Force and EKF for Two-Body WECs

The excitation force on the spar and the excitation force on the floater are estimated using the models described in section 2.1.4. The floater and spar excitation forces are then used to find the relative excitation forces using the dynamics described developed in section 2.2. The relative excitation forces are then combined before being entered into the "relative" EKF, from which the combined excitation force, frequency and amplitude estimates are output ($\phi_c$, $\omega_c$ and $A_c$ respectively). The flow of inputs and outputs is presented in Fig. 4. Note that for the (non-relative) excitation force ($F_{ExF}$ and $F_{ExS}$) the non-linear drag (see sub-section 2.2.4) can be directly computed without requiring approximation, which is only required for the relative excitation force estimates ($F_{ExFR}$ and $F_{ExSR}$).

### 2.2.4. Drag force modelling

For the two body WEC modelled in this work the drag force of the spar is required to be modelled. The drag force ($F_D$) is non-linear and can be modelled by

$$F_D = \frac{1}{2}\rho A V |V| \tag{37}$$

where $\rho$ is the density of the fluid, $A$ is the reference area, $C_D$ is the coefficient of drag, and $V$ is the velocity of the body. For the calculation of the plant and the calculation of $B$ this force must be linearised about a sensible operating point. During operation the speed of the PTO necessarily changes and a hence a method of dynamically adjusting the WEC model to account for the associated non-linearity is desirable. Methods such as those used in [14, 15], that maintain extended local linear equivalence, are suggested as possible implementations of such a non-linear model, although the development of such models is considered outside the scope of the work presented here. Instead, a single

PTO speed is chosen for the linearisation of the model for use in the estimates of relative excitation. For the majority of the work presented, the PTO speed for the linearisation is set at $1m/s$. Where a different value is used this is explained in the text. The variation in admittance with changing velocity for linearisation is shown in Fig. 5.

### 2.3. Limits

Constraint of the PTO position and velocity was presented in [5] and the methodology is used here and extended to include acceleration limits. The combined position, velocity, and acceleration constraints are referred to as movement constraints. The WEC reference velocity is given by:

$$v_{ref}(\omega) = \frac{F_{ex}(\omega)}{H(\omega)} \tag{38}$$

and assuming that the excitation force is a narrow-band harmonic process with amplitude $A$, the complex magnitude of the velocity, $\hat{V}$, and position, $\hat{X}$, can be expressed as:

$$\hat{V} = \frac{A}{H}e^{j\phi} \tag{39}$$

$$\hat{X} = \frac{\hat{V}}{j\omega} = \frac{Ae^{j\phi}}{j\omega H} \tag{40}$$

When $\hat{X}$ is constrained:

$$\hat{X} = \frac{\hat{V}}{j\omega} < X_{lim} \rightarrow |\hat{V}| < X_{lim}\omega \rightarrow \frac{A}{H} < X_{lim}\omega \rightarrow \frac{1}{H} < \frac{X_{lim}\omega}{A}$$

which gives an upper limit of the function $1/H$. Limits on the velocity and the acceleration can be applied using the same reasoning, with each giving an upper limit of $1/H$. Considering velocity:

$$|\hat{V}| = \frac{A}{H} < V_{lim} \rightarrow \frac{1}{H} < \frac{V_{lim}}{A} \tag{41}$$

Considering acceleration:

$$\hat{A}_{cc} = \hat{V}_{lim}j\omega \tag{42}$$

$$|\hat{V}|\omega = \frac{A}{H} < A_{cclim} \rightarrow \frac{1}{H} < \frac{A_{cclim}}{A\omega} \tag{43}$$

As more than one limit may be effective at any one time, the minimum value of $\frac{X_{lim}\omega}{A}, \frac{V_{lim}}{A}$, and $\frac{A_{cclim}}{A\omega}$ is multiplied by the excitation force to produce the reference velocity that complies with the constraints. It should be noted that the formulation of the constraints given here assumes that the wave frequency and amplitude are known and correct but are normally estimated. As such, the constraints should not be used as hard constraints and an error margin must be considered.

### 2.4. Force constraints

In addition to the limits on position, velocity, and acceleration, the command force must also be limited as PTOs have maximum and minimum forces that they can safely deliver. Whilst a simple saturation could be applied to the output from the controller, such a limit may lead to integral wind up if there is integration in the controller. To avoid integral wind up, a discrete form of anti-wind up is used. First, the transfer functions in the controller are defined in discrete form, such that:

$$F_s(s) \rightarrow F_z(z) = \frac{n(z)}{d(z)} = \frac{a_{nz}^{-n} + a_{n-1}z^{n-1} + \cdots + a_1z^{-1} + a_0}{b_{mz}^{-m} + b_{m-1}z^{-(m-1)} + \cdots + b_0z^{-1} + 1} \tag{44}$$

$$F_z(z) - a_0 = z^{-1}\frac{m(z)}{d(z)} = z^{-1}G_z(z) \tag{45}$$

so,

$$f_k = g_{k-1} + a_0 u_k \tag{46}$$

In this way, the output of the function $F$ at time step $k$ is equal to the output of function $G$ at the time step $k-1$ plus a constant times the input at time step $k$. If the resulting force exceeds the maximum force, it is very easy to recalculate the limited input to the whole controller. It should be noted that, whilst not demonstrated here, the same methodology could be used to limit the rate of change of force if it was of concern.

### 2.4.1. Eliminating Drift

It is found that when the force limit is applied the mean displacement of the device can drift substantially from the desired level during irregular wave simulations. In order to prevent this slow movement away from the desired depth, an addition is made to the controller that acts on the integral of the measured speed such that the error $\epsilon = v_{ref} - v$, is replaced by:

$$\epsilon = v_{ref} - v - \frac{kv}{s} \tag{47}$$

where $k$ is a small number of the order of 0.01 to 0.05. The addition of the $\frac{kv}{s}$ term with a small $k$ can be viewed as adding a very slow control action acting on mean displacement. Keeping the gain low prevents the addition from interfering with the controller action as the displacement component only acts at very low frequencies. The impact on power capture is negligible.

## 3. Controller Design

In this section controllers are designed for two example WECs. The WECs are two of the exemplar devices from the IMPACT toolbox [12], referred to within the IMPACT toolbox as WEC 2 and WEC 3. WEC 2 is a bottom fixed single-body submerged WEC. Both WECs are large utility scale (multi-megaWatt) devices. In this section, the site conditions considered for WEC power generation are introduced in subsection 3.1, the design of the controller for WEC 2 is discussed first in subsection 3.2, whilst the design of the controller for WEC 3 is discussed in subsection 3.3. Where limits are applied, the PTO force is limited to $3.5MN$, the PTO position is limited to $4.5m$, the PTO velocity is limited to $3m/s$, and the PTO acceleration is limited to $2m/s^2$.

### 3.1. Site conditions

When designing a controller for a WEC it is important to take into account the conditions of the site. In this case the site chosen is an area of the sea to the south west of Wales, with wave measurements collected over 18 months from the Celtic Sea Wave 31 radar [16]. Based on this site, a design envelope for power production in waves of periods 6s to 16s and wave heights of 1m to 6m was defined (see Fig. 6).

### 3.2. Single body WEC

A WEC model is created using the IMPACT toolbox [12], specifically using the Cummins equation (equation 1). The values for the $A(\omega)$ and $B(\omega)$ matrices are generated via the Boundary Element Method (BEM) code NEMOH [17]. Using the methodology of section 2, the intrinsic impedance of the WEC is calculated for a range of frequencies. The phase and magnitude can hence be calculated for a range of frequencies, which is shown in Fig. 7a. Through the use of the methodology described in [13], a linear approximation of the dynamics can also be made. In this case an approximation of the seventh order in the numerator and of the eighth order in the denominator is required to give a good estimate and is also shown in Fig. 7a and is given by,

$$\frac{1.2171 \times 10^{-7}(s + 21.36)(s + 0.02383)(s + 0.02327)}{(s + 7.924)(s + 0.02341)(s + 0.02286)(s + 0.001782)} \times \frac{(s^2 + 0.09822s + 0.64)(s^2 + 0.4412s + 0.8349)}{(s + 0.001781)(s^2 + 0.1057s + 0.6322)(s^2 + 0.5802s + 1.264)} \tag{48}$$

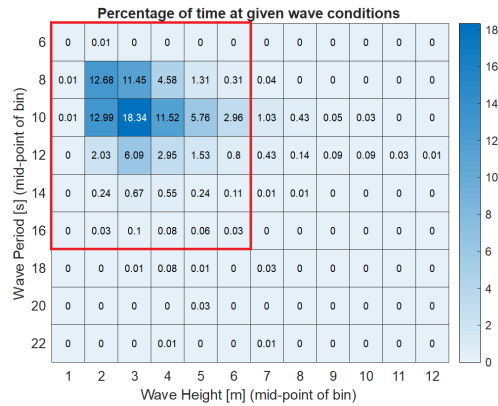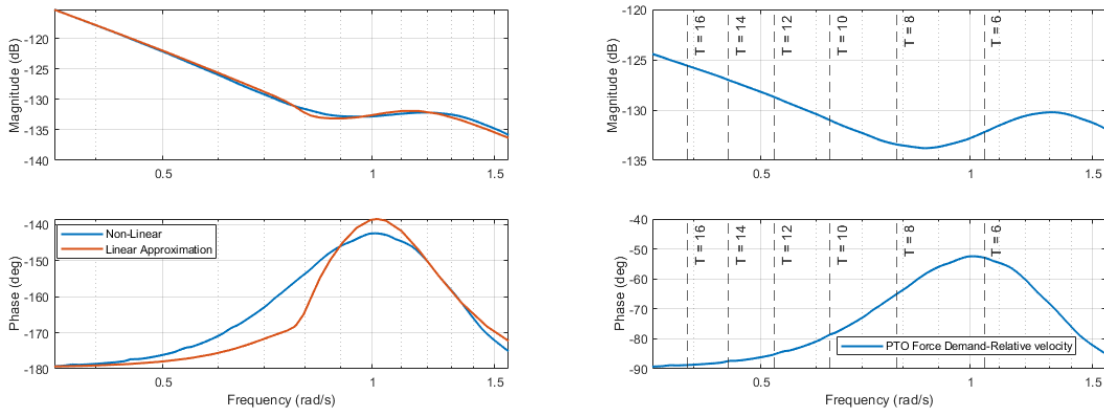It is this linear relationship that is used to estimate the excitation force based on the movement of the WEC.

Figure 6: Probability (%) of sea state conditions for the chosen site. The operational conditions are highlighted n the red box and encompass 97.4% of the conditions (Celtic Sea Wave 31 on the edge of the Bristol Channel south west of Wales - data from [16])



(a) Non-Linear dynamics based on the Cummins equation (blue) and the linear approximation (red) of excitation force to position, used for estimating the excitation force

(b) Non-Linear dynamics based on the Cummins equation of excitation force to velocity, used for controller design

Figure 7: Non-linear dynamics from force to position (a) and from force to velocity (b) for the one-body WEC

Fusco and Ringwood describe a methodology for designing a controller that uses the intrinsic impedance of the WEC in the formulation such that,

$$K(s) = \frac{Q(s)}{1 - Q(s)/Z_i(s)} \tag{49}$$

where $Q(s)$ is a filter designed by the control engineer [5]. Whilst this approach is useful for simple WEC dynamics, for a system such as that of WEC 2, where the intrinsic impedance is eighth order, the controller becomes highly complex. Instead, standard control design methods can be used to design a simpler controller using the non-linear dynamics for excitation force to velocity shown in Fig. 7b.

The control goal is to design the controller such that the closed loop dynamics have close to zero dB magnitude and close to 0 degrees phase across the operational range. The operational range in this case is set as between periods of 6s and 16s (i.e. between frequencies of approximately 0.4 and 1.05 rad/s). Because of these range of frequencies, there is no need of an integral action to remove the steady state error. In addition, for WEC 2 there is a very low frequency pole and adding integral action to the controller greatly reduces the phase of the closed loop system. The phase loss should be minimised for the bandwidth of the wave frequencies as any difference in phase shifts the controller away
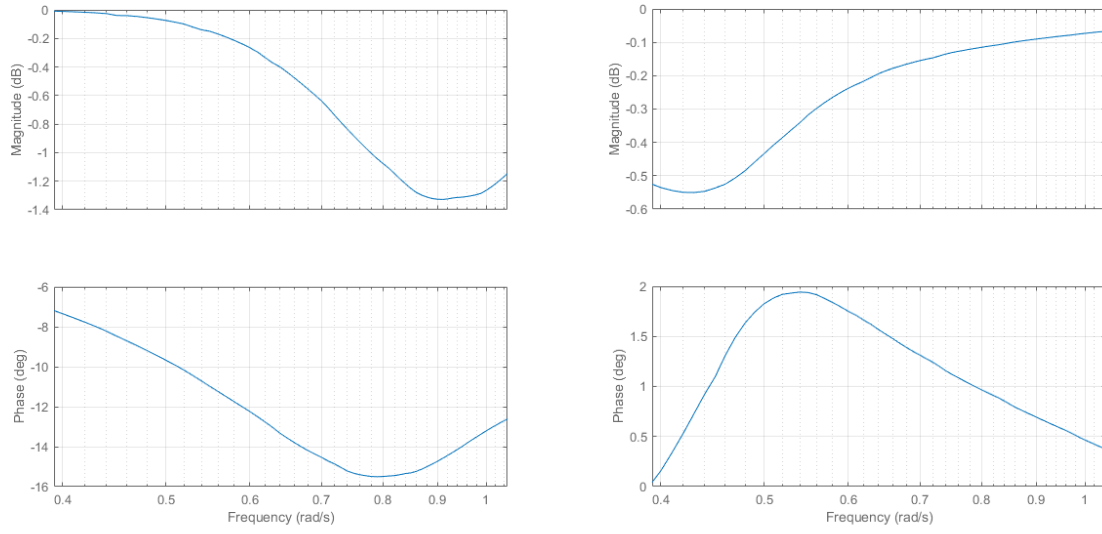
(a) Closed loop dynamics of plant and controller for one-body body WEC - response within the operational range shown

(b) Closed loop dynamics of plant and controller for two body WEC (IMPACT Exemplar WEC 3) - response within the operational range shown with a controller gain of $1 \times 10^8$

Figure 8: Closed loop Bode plots for the one-body WEC (a) and the two-body WEC (b)

from the impedance matching phase of the reference velocity. Using a controller of the form,

$$7.038 \times 10^7 \frac{s + 0.00589}{(s + 0.00916)(s + 4.616)} \tag{50}$$

the closed loop dynamics are as per Fig. 8a.

### 3.3. Two body WEC

For a two-body device the model of the dynamics discussed in section 2.2 must be utilised. The controller can then be designed using the combined floater and spar model (including body to body interactions) with the same goals as for single-body devices. The transfer function from velocity to force produced for a two-body device (the exemplar "WEC-3" of the IMPACT toolbox) is,

$$\frac{(s + 1.315)(s + 1.244)(s^2 + 0.1433s + 0.02839)(s^2 + 0.3171s + 1.679)(s^2 + 0.005061s + 2.861)}{s(s + 7.856)(s + 2.924)(s + 1.083))(s^2 + 0.1858s + 0.2147)(s^2 + 0.001224s + 2.719)} \tag{51}$$

Looking at the closed loop plant and controller dynamics it is clear that a simple gain suffices for control across the frequencies of interest. A gain of $1 \times 10^8$ is selected. The closed loop dynamics are shown in Fig. 8b.

### 3.3.1. Reduced gain for two body WEC

When running simulations for the two body WEC, the optimum gain is found by experiment to be lower than the expected value. Such a result is initially confusing as the controller is effectively minimising the error of the PTO velocity from the reference speed and so, as long as stable, the higher the gain the better the performance would be expected to be. However, consideration of the detail of the controller reveals the reason for the discrepancy. A simplified diagram of the controller and plant for the system is shown in Fig. 9, where $V_R$ is the reference speed, $C$ is the controller (in this case a gain), $F_E$ is the excitation force, and $P$ is the plant. It follows that,
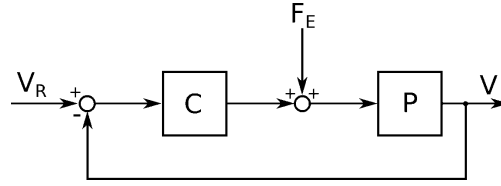
$$V = P(F_E + C(V_R - V)) = PF_E + PC(V_R - V) \tag{52}$$

Figure 9: Simple control diagram

$$V(1 + PC) = PF_E + PCV_R \tag{53}$$

$$V = \frac{P}{1 + PC}F_E + \frac{PC}{1 + PC}V_R \tag{54}$$

If the gain of C is high, the term $\frac{P}{1+PC}$ gets very small. The velocity will follow the reference but the effect of the excitation force on the velocity is masked by the PTO force. A modification of the controller gain can be made to take into account the effect of the closed loop.

$$V = \frac{P}{(1 + PC)}(F_E + CV_R) = \frac{PC}{(1 + PC)}\left(\frac{F_E}{C} + V_R\right) \tag{55}$$

As the reference speed is given by,

$$V_R = \frac{F_E}{2B} \tag{56}$$

so,

$$V = \frac{PC}{(1 + PC)}\left(\frac{2B}{C} + 1\right)V_R = XV_R \tag{57}$$

The $PC/(1 + PC)$ term is the closed loop controller transfer function, which tends to 1 for infinite gain of $C$. The $2B/C$ term tends to 0 for infinite gain and so $X$ tends to 1 and $V$ tends to $V_R$ as expected. For lower gains of $C$ however, $X$ does not equal 1, but is a function of $B$. As $V = XV_R$, to make the controller correctly control to the reference velocity, the reference velocity input must be divided by X so,

$$V = \frac{XV_R}{X} = V_R \tag{58}$$

Note that experimentation has found that the optimum gain does not vary with wave height or frequency and so it does not need to be varied. For the simulations in this work a value of $8.8041 \times 10^6$ was used.

### 3.4. Linear Damping Controller

In order to provide a comparison against which to assess the OVT controllers, linear damping controllers are also designed. Linear damping uses a set gain such that the force response of the PTO is proportional to the velocity of the PTO, that is,

$$F_U = K_{LD}V \tag{59}$$

where $K_{LD}$ is set at the optimum value for the dominant site wave period (10s).

## 4. Results

In subsection 4.1 the results of simulations of the single body WEC are discussed. The results of the two body WEC simulations are discussed in subsection 4.2. For each WEC, 1000 second WEC-Sim simulations are conducted using irregular waves over a wave period range of 6s to 16s in steps of 2s and with wave heights 1m to 6m in steps of 1m. The first 400s are discarded as transients. The average power for each wave height and period combination is found and then, using the probability distribution shown in Fig. 6, the average energy capture for an example site is calculated. Simulations using two different strategies are compared - passive linear damping (PLD) and optimal velocity tracking (OVT). For both WECs, simulations are conducted with a force limit of $3.5MN$, a displacement limit of $4.5m$, a velocity limit of $2ms^{-1}$ and an acceleration limit of $5ms^{-2}$. The limits are based on typical estimates of PTO capabilities [18]. PTO efficiency is not considered in this work but would be an interesting addition for future work, perhaps building on preliminary work completed in [12, 19].
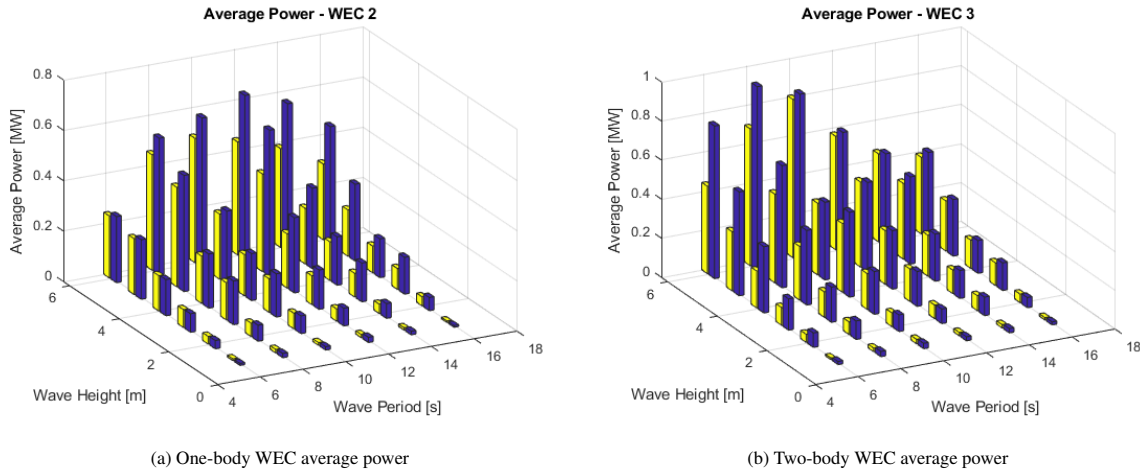
(a) One-body WEC average power                      (b) Two-body WEC average power

Figure 10: Average power for each wave height and wave period combination for (a) one body WEC and (b) two-body WEC

### 4.1. Single Body WEC

#### 4.1.1. Comparison of Average Power Capture

The average power capture (total energy divided by simulation time) for the single body WEC for a range of wave heights and wave periods and with PLD and OVT is shown in Fig. 10a. OVT typically shows a significant increase in the average power output of the WEC, particularly at higher wave periods (above 10s). The improvement in performance of a WEC in terms of energy capture is dependent upon the wave climate and so some assumptions have to be made. Assuming a wave climate as is shown in Fig. 6, and that the WEC is operated in the red highlighted region, OVT shows improvements in energy capture of 23% compared to PLD. It should be noted that the site chosen has a narrow distribution of wave periods and that the WEC is not as peaked in its response as other WEC designs may be (such as WEC 1 from the IMPACT toolbox). A more peaked resonant frequency and a broader distribution of wave periods would see a larger increase in energy capture for the WEC with OVT compared to PLD, as the WEC would operate more often further from the optimum for PLD where the benefits of OVT would be greater.

#### 4.1.2. Comparison of Forces

Plots of the PTO force against PTO speed and PTO force against time for simulations with a wave height of 3m are shown in Fig. 11a and for a wave height of 6m in Fig. 11b. PLD does not require the force of the PTO to be limited except in very large waves (6m) and at high wave periods (14s and 16s). As would be expected, the plot of force against PTO speed shows a linear relationship with a constant gradient set by the PLD gain. For OVT operation it is clear that the relationship between force and speed is far from linear, as would be expected given the phase relationship. At high periods the phase is close to 90 degrees and so the peak force is at close to zero velocity. In some cases (notably for the 16s period simulation with wave height 6m in Fig. 11b) the PTO speed limits are exceeded. There are two reasons for the PTO velocity exceeding the limits. Firstly, there will often be a small error in tracking the speed, causing the velocity limit to act a s a "soft" rather than a "hard" limit. Secondly, limiting the velocity of the WEC may, in some cases, require larger PTO forces than the force limit allows. In these cases the PTO velocity limit will be further exceeded.

### 4.2. Two Body WEC

For the two body WEC, linearisations at 0.15m/s, 0.5m/s, and 1m/s PTO speed are used for controller design and simulations run with all of them. For each combination of wave period and wave height the results for the linearisation with the best energy capture is used.

(a) One-body WEC PTO force 3m waves
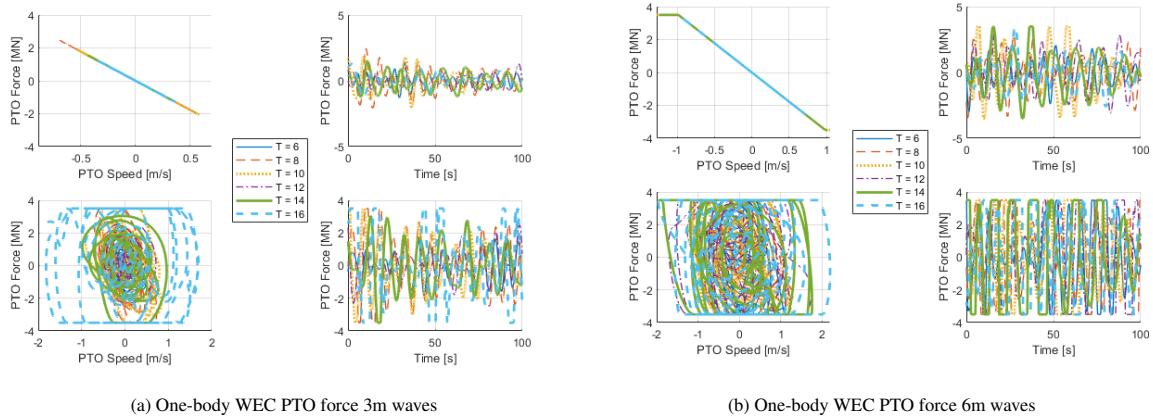
(b) One-body WEC PTO force 6m waves

Figure 11: PTO Force and PTO speed for the one-body WEC. in each sub-figure the left hand plots shows the PTO force against PTO speed for PLD (top plot), and OVT (bottom plot). The right hand plot shows the time series of PTO force. Sampled from the last 100s of simulations
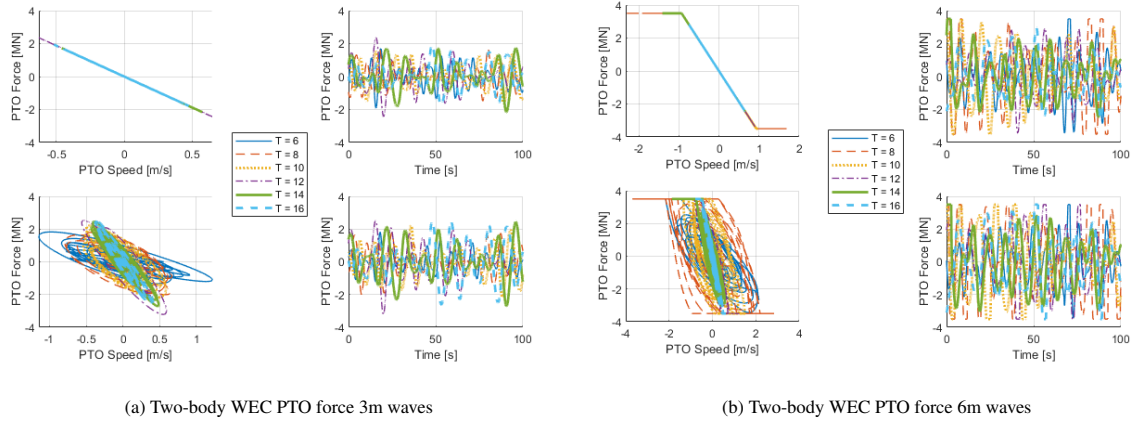


(a) Two-body WEC PTO force 3m waves

(b) Two-body WEC PTO force 6m waves

Figure 12: PTO Force and PTO speed for the two-body WEC. in each sub-figure the left hand plots shows the PTO force against PTO speed for PLD (top plot), and OVT (bottom plot). The right hand plot shows the time series of PTO force. Sampled from the last 100s of simulations

### 4.2.1. Comparison of Energy Capture

For the OVT simulations, the improvement in energy capture compared to PLD was 20%, similar to the improvements for the one-body device. This is as expected, as WEC 3 has a similarly broad response to WEC 2, albeit with the a larger divergence from the phase and gain of the dominant site period occurring at periods greater than 12s (compare Fig. 7b and Fig. 5). For site conditions with a broader spread of wave periods the difference in total energy capture from using different linearisations is likely to be larger. Typically, for higher periods the lower linearisation speed of 0.15m/s yielded the most energy. At lower periods higher linearisations up to 1m/s yielded the most energy. Because of the narrow of wave periods for the site, using the linearisation best suited to a period of 10s (the 1m/s linearisation) across the whole operational envelope only reduced energy capture by 1%. For the two-body WEC, the greatest improvement in energy capture compared to PLD is at low periods. The phase at these periods is similar to that at the dominant period of 10m/s but the difference in gain is large. At high periods, the difference in gain is smaller, and, although there is a clear difference in phase, the phase change is towards 0 degrees, i.e. back towards optimum for linear damping. As such, the gains in energy at higher periods compared to linear damping are lesser.

### 4.2.2. Comparison of Forces

Plots of the PTO force against PTO speed and PTO force against time for simulations with a wave height of 3m are shown in Fig. 12a and for a wave height of 6m in Fig. 12b. PLD does not require the force of the PTO to be
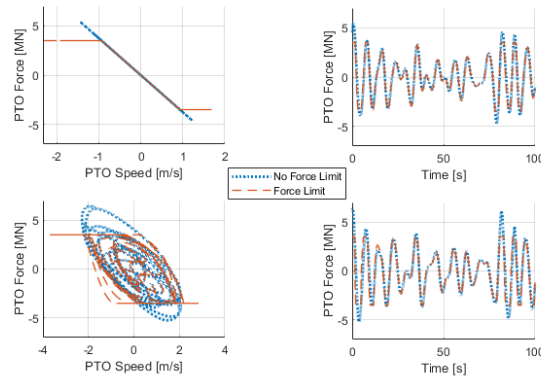
Figure 13: WEC 3 PTO force - The left hand plots shows the PTO force against PTO speed for PLD (top plot), and OVT (bottom plot) with and without the limit on PTO force. The right hand plot shows the time series of PTO force with and without the force limit. Sampled from the last 100s of simulations with wave height of 6m and period of 8s

limited except in very large waves (6m). The phase difference between speed and force is generally lower than for the one-body WEC, leading to more elongated ovals on the force-speed plots. The difference in gain at each period is clearly observable in Fig. 12a, where the ovals for periods of 6s and 8s have a much different gradient compared to the other simulations, whose gradients are more similar.

In Fig. 12b a clear breach of the velocity limit is seen for the simulation with 8s period. The breach of the limit is driven predominantly by the force limit, which prevents the PTO from exerting enough force to keep the PTO velocity within the limit. Fig. 13 shows the simulation both with a force limit and without. It is clear that although the velocity limit is breached slightly when there is no force limit, the breach is much worse when the limit is enforced. A method of limiting the force that can account for such eventualities is an area for future work.

## 5. Conclusions

In the work presented here an Optimal Velocity Tracking (OVT) control methodology for application on both one-body and two-body wave energy converters (WECs) that includes limits on the PTO has been detailed. The control methodology was applied to both one and two-body exemplar WECs, with an improvement in energy capture of 23% compared to typically used passive linear damping (PLD) techniques for the one-body device and improvements of 20% for the two-body device.

The work presented shows that OVT can be successfully implemented on both one and two body WECs, including limits on the movement and the force, with similar improvements in performance for both WEC types. The WECs in this study have broad bandwidth dynamics compared to some point absorbers and the site chosen has a fairly narrow distribution of wave periods. A WEC with more peaked dynamics and a site with a broader distribution of wave periods would see greater benefit from OVT control.

The work highlights several areas for development in future work. These are,

- Improved, non-linear representation of the drag forces

- Development of a force limitation method that maintains the velocity limit, even in extreme conditions

- A method to account for non-linear efficiencies in the PTO

Finally, a highly interesting area for future work would be the implementation of the OVT control methodology in a wave tank or at sea test at either part or full scale.

## Acknowledgements

## References

[1] J. Scruggs, P. Jacob, Harvesting ocean wave energy, Science 323 (5918) (2009) 1176–1178.
[2] B. Drew, A. R. Plummer, M. N. Sahinkaya, A review of wave energy converter technology (2009).
[3] J. Hals, J. Falnes, T. Moan, A comparison of selected strategies for adaptive control of wave energy converters, Journal of Offshore Mechanics and Arctic Engineering 133 (3) (2011).
[4] J. Falnes, A. Kurniawan, Ocean waves and oscillating systems: linear interactions including wave-energy extraction, Vol. 8, Cambridge university press, 2020.
[5] F. Fusco, J. V. Ringwood, A simple and effective real-time controller for wave energy converters, IEEE Transactions on Sustainable Energy 4 (1) (2013) 21–30. doi:10.1109/TSTE.2012.2196717.
[6] N. Faedo, S. Olaya, J. V. Ringwood, Optimal control, MPC and MPC-like algorithms for wave energy systems: An overview, IFAC Journal of Systems and Control 1 (2017) 37–56. doi:10.1016/j.ifacsc.2017.07.001.
[7] T. Kamio, M. Iida, C. Arakawa, Numerical simulation and optimization of a wave energy converter for the Izu Islands sea in Japan, Proceedings of the International Conference on Offshore Mechanics and Arctic Engineering - OMAE 9A (2014) 1–7. doi:10.1115/OMAE2014-23544.
[8] M. Richter, M. E. Magana, O. Sawodny, T. K. Brekken, Nonlinear model predictive control of a point absorber wave energy converter, IEEE Transactions on Sustainable Energy 4 (1) (2012) 118–126.
[9] M. Richter, M. E. Magaña, O. Sawodny, T. K. Brekken, Power optimisation of a point absorber wave energy converter by means of linear model predictive control, IET Renewable Power Generation 8 (2) (2013) 203–215.
[10] S. Olaya, J.-M. Bourgeot, M. Benbouzid, On the generator constraint design of a wave energy converter at a pre-sizing stage, 2015.
[11] K. Ruehl, C. Michelen, S. Kanner, M. Lawson, Y.-H. Yu, Preliminary verification and validation of wec-sim, an open-source wave energy converter design tool, in: ASME 2014 33rd International Conference on Ocean, Offshore and Arctic Engineering, American Society of Mechanical Engineers Digital Collection, 2014.
[12] A. Stock, C. Gonzalez, D. Robb, Final Stage 2 Project Report - IMPACT, Tech. rep., SgurrControl, Glasgow (2018).
     URL https://library.waveenergyscotland.co.uk/
[13] D. Valério, M. D. Ortigueira, J. Sá da Costa, Identifying a transfer function from a frequency response, Journal of computational and nonlinear dynamics 3 (2) (2008).
[14] D. W. Thompson, Mitigating Size Related Limitations in Wind Turbine Control, Ph.D. thesis, University of Strathclyde (2018).
[15] D. J. Leith, W. E. Leithead, Appropriate realization of gain-scheduled controllers with application to wind turbine regulation, International Journal of Control 65 (2) (1996) 223–248.
[16] CEFAS, Cefas wavenet wave monitoring network (2020).
     URL http://wavenet.cefas.co.uk
[17] A. Babarit, G. Delhommeau, Theoretical and numerical aspects of the open source bem solver nemoh, in: Proceedings of the 11th European Wave and Tidal Energy Conference, 2015.
[18] Trident Energy, PowerPod Technical Datasheet, Tech. rep., Trident Energy (2014).
[19] A. Stock, N. Tom, C. Gonzalez, Adapting Optimal Velocity Tracking Control To Account for WEC Constraints and Power-Take-Off Efficiencies, in: Internation Federation of Advanced Control (IFAC), Berlin, 2020.